Dynamic strain measurements of marine propellers under non-uniform inflow

Jin Tian[1], Paul Croaker[2], Zhiyi Zhang[1] and Hongxing Hua[1]
[1]Institute of vibration, shock and noise, Shanghai Jiao Tong University, 800 Dongchuan Road, Shanghai 200240, P. R. China
[2]School of Mechanical and Manufacturing Engineering, UNSW Australia, Sydney, NSW 2052, Australia
E-mail: tianjinsjtu@sjtu.edu.cn

Abstract. An experimental investigation was conducted to determine the dynamic strain characteristics of marine propellers under non-uniform inflow. Two 7-bladed highly skewed model propellers of identical geometries, but different elastic characteristics were tested at various rotational speeds and free stream velocities in the water tunnel. Two kinds of wire mesh wake screens located 400mm upstream of the propeller plane were used to generate four-cycle and six-cycle inflows. A laser doppler velocimetry (LDV) system located 100mm downstream of the wake screen plane was used to measure the axial velocity distributions produced by the wake screens. Strain gauges were bonded onto the propeller blades in different positions. A customized underwater data acquisition system which can record data off-line was used to record the dynamic strain. The results show that the frequency properties of the blade dynamic strain are determined by the harmonics of the inflow and that the stiffness of the propeller has an essential effect on the dynamic strain amplitudes.

Keywords: dynamic strain; propeller blade; Laser Doppler Velocimetry.

1.Introduction

The fluctuating forces of propeller blades under non-uniform inflow can lead to unwanted underwater noise and structural fatigue. Many researchers have studied these unsteady forces through dynamic strain measurements. Zetterlind et al. [1] conducted the fatigue testing of a composite propeller blade which was subjected to a constant axial load and a cyclic bending load using fiber-optic strain sensors. In their experiments, both static and dynamic data between fiber-optic sensors and co-located resistive gages showed good correlation. Seaver et al. [2] measured the dynamic strain using embedded arrays of fiber Bragg grating sensors in composite propeller blades when the propeller was being tested in a water tunnel. The results showed that large strain variations depended on the location of the blade in the non-uniform flow field. Liu et al. [3] built a fiber optic sensor system for strain and pressure measurements on a rotating blade. This system was based on low coherent interferometry, which is insensitive to wavelength or intensity induced noise, allows high sensitivity, higher resolution, and fast demodulation. Swithenbank et al. [4] performed the dynamic strain measurements of Propeller 4381 in crashback conditions in the 36-inch water tunnel at the Naval Surface Warfare Center. The results showed that the maximum unsteady strains were at up to 2.5 times the mean strain on the blade.

In general, far fewer dynamic strain measurements have been carried out for marine propellers than for turbine machines or wind turbines. The experimental methods developed for rotors that operate in air can also be used for marine propellers [5-10].

The objective of this paper is to investigate dynamic strain of propeller blades under non-uniform inflows. Furthermore, the effect of elastic characteristics on blade dynamic strain response was studied. A flexible (made of plastic) propeller and a rigid propeller (made of bronze) of identical geometries were tested under various excitation frequencies which were induced by four-cycle or six-cycle wake screens. Data from strain gauges on the propeller blades quantified the vibratory strain amplitudes and excitation frequencies induced by the wake screens. The dynamic strain amplitudes under different inflows were analyzed to gain insight into the structure responses induced by the non-uniform inflows.

2.Experimental set-up and procedure

The experiments were conducted in the water tunnel at Shanghai Jiao Tong University, which has a 700 mm×700 mm square test section and a length of L_w=10.6 m and can produce a maximum flow velocity of 5 m/s. Figure 1 shows the experimental set-up in the water tunnel and includes the model propeller, the shaft system and the wake screen. The propeller is driven by a DC motor, which allows a maximum rotational speed of 1500 rpm. Two model propellers of identical geometries, but different materials were used in the tests. Four-cycle and six-cycle wake screens were used to generate two kinds of non-uniform inflows. Dynamic strain of these two propellers was measured at various tunnel speeds and rotational speeds under non-uniform inflow. During the tests, the two propellers and two wake screens were swapped to keep that the two propellers have the same test cases.

2.1. Model propellers

The propeller geometries consisted of 7 highly skewed blades with a diameter of 250 mm. The detailed dimension of the propeller geometry is listed in Table 1.

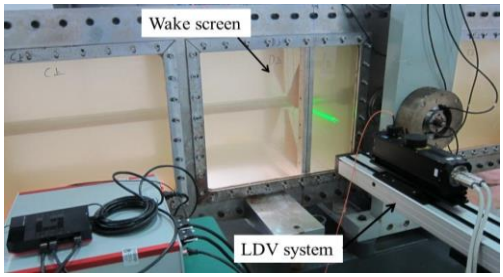

Figure 1. Experimental set-up in water tunnel.

Table 1. Propeller parameters.

Model propeller parameters	
Diameter	D=250mm
Number of blades	7
Pitch ratio	1.1
Hub ratio	0.2

2.2. Wake screens and LDV system

Wire mesh screens located 400 mm upstream of the propeller plane were used to generate the four-cycle and six-cycle inflows. This technique was an extension of that used in Jessup's tests [11]. A coarse base screen (25 mm×25 mm mesh size) was stretched and soldered on to a steel frame which was mounted on to the water tunnel wall. Sections of dense screen (2 mm×2 mm mesh size) were overlapped over the base screen to construct specific patterns. Several overlays were used to create a more sinusoidal wake pattern. Figure 2 shows the schematics for the four-cycle and six-cycle wake screens. Figure 1 shows the four-cycle wake screen in the water tunnel.

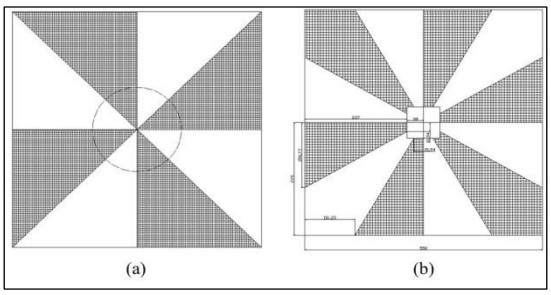

Figure 2. The schematics of wake screens. (a) four-cycle; (b) six-cycle.

A laser doppler velocimetry system (ILA fp50 shift) was located 100 mm downstream of the wake screen plane as shown in Figure 1. This LDV system was used to measure the axial velocity distributions produced by the wake screens.

2.3. Strain gauges and underwater data acquisition system

The strain gauges were mounted at 0.6R and 0.8R on the suction side of two different blades. The strain gauges were in three directions (0 degrees, 45 degrees and 90 degrees). The 90 degree strain gauge has the same direction as the blade reference line. A potting compound was used to waterproof the strain gauges. Figure 3 shows the strain gauges which were mounted on the bronze propeller blades. A special purpose offline underwater data acquisition system was built and assembled with the hub to record the strain signal. With the lithium battery, the data acquisition system can work offline for more than three hours.

Figure 3. Strain gauges on the bronze propeller blades.

2.4. Test cases

A series of test cases were designed to investigate the dynamic strain properties of the blades. Initially, measurements were carried out at various tunnel speeds and rotational speeds without any wake screen. The purpose of these tests was to study the influence of the propeller-shaft system. After these initial tests, measurements were conducted with the propeller rotating in the four-cycle wake field. The final set of measurements was performed for the propeller rotating in the six-cycle wake field. For each of these test cases, the measurements lasted approximately 100 s. The bronze and plastic propellers were both tested for all cases. A sampling frequency of 1000 Hz was used for the measurements.

3.Experimental results and discussion

In what follows, results of the axial velocity distribution of different wake screens, strain response of different inflows and the effect of the propeller's elastic properties on strain response are discussed and compared.

3.1. LDV measured axial velocity distribution

Figure 4 shows the time-averaged normalized axial velocity (U_{ax}/U) at U=1 m/s. U is the tunnel speed measured by the ultrasonic flowmeter. U_{ax} is the time-averaged axial velocity measured by the LDV system. Figures 4(a) and (b) are the normalized axial velocity distributions with four-cycle and six-cycle wake screens, respectively. The velocity distributions indicate that the wake screens are successful at generating four-cycle and six-cycle inflows. When the propeller was operating in these non-uniform inflows, the blades were subjected to the fluctuating forces. In the present experiments, strong fluctuating forces were expected to produce a measurable strain response.

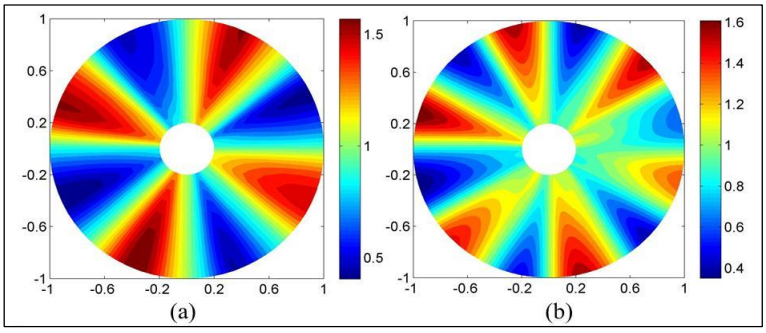

Figure 4. Measured time-averaged normalized axial velocity (U_{ax}/U) at U=1 m/s. (a) four-cycle distribution; (b) six-cycle distribution.

3.2. Vibratory strain response without wake screens

Initially, the baseline dynamic strain response was measured without any wake screen. Figure 5 shows the strain frequency spectra of the bronze propeller for multiple rotational speeds. The axial passing frequency (APF Hz) is defined as the shaft rotational frequency. Figure 5 reveals that the dominant frequencies occur at the APF and its harmonics. The harmonics were found to produce different amplitude strains for different advance coefficients. The frequency is linked to the rotational speed and does not change with the tunnel speed. These properties are in good agreement with Swithenbank's experiments [4]. These peaks can be caused by imbalances in any part of the system such as in the propeller or the shaft or any hydrodynamic non-uniformity. The plastic propeller exhibited the same dynamic strain characteristics as the bronze one. The amplitudes at APF of the plastic propeller are larger than that of the bronze propeller.

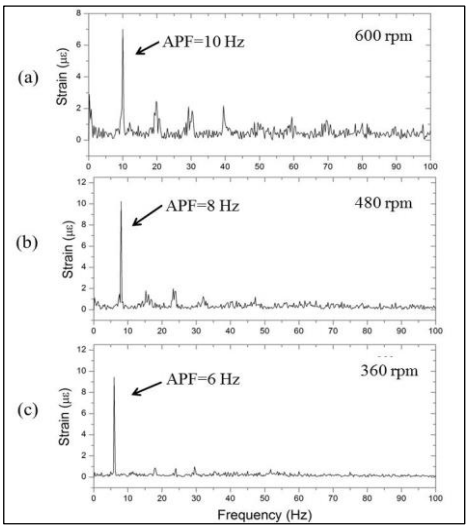

Figure 5. Strain frequency spectra with bronze propeller, uniform inflow, U=0 m/s, 45 degree strain gauge, 0.6R. (a) 600 rpm; (b) 480 rpm; (c) 360 rpm.

The results show that the strain gauges of different directions and at different radial position have the same frequency characteristics. So the data from 45 degree strain gauge at 0.6R is presented in the following analysis.

3.3. Vibratory strain response with four-cycle wake screen

As stated earlier, the strain gauges were located at 0.6R, 0.8R and in three directions (0 degrees, 45 degrees and 90 degrees relative to the blade mean chord line). So it is necessary to study the difference between different positions and directions. Figure 6 shows the frequency spectra of the three strain gauges for the plastic propeller in the four-cycle inflow at 600 rpm (APF=10 Hz). Small peaks at APF and its harmonics can still be seen, however the maximum peak now occurs at 4APF (40Hz). These results are noticeably different from the results obtained for a uniform inflow. The strong peak at 4APF corresponds to heavy loading conditions when the propeller blades pass through each of the four low axial velocity regions shown in Figure 4(a). These single blade forces with a frequency of 4APF have also been predicted using numerical methods [12, 13]. Attention must be paid to these fluctuating forces as they excite the propeller and radiate unwanted underwater noise.

Figure 6 also reveals that the three strain gauges (0 degrees, 45 degrees and 90 degrees) have the same frequency characteristics. The data from 45 degree strain gauge which has the maximum amplitude at 4APF was used in the following analysis. The reason why the 45

degree strain gauge has the maximum amplitude is that the deformation of the blade contains both bend and twist.

Figure 7 shows the frequency spectra at different radial locations. The strain gauges at 0.6R and 0.8R have the same frequency characteristics but different amplitudes. The amplitude at 0.6R is approximately twice as large as the amplitude at 0.8R. The results reflect the stress distribution of a single blade which is similar to a cantilever beam with stress increasing towards the hub. For the sake of brevity only the strain measurements obtained at 0.6R will be used in the following discussion. Figures 8 and 9 show the strain frequency spectra at multiple rotational speeds for the plastic and bronze propeller, respectively. The spectra have maximum peaks at 4APF and the peak amplitudes of the plastic propeller are approximately twice as large as the bronze propeller's peak strain.

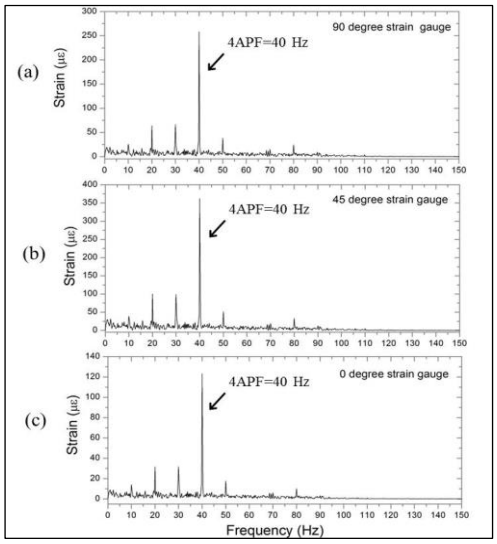

Figure 6. Strain frequency spectra in different directions, with plastic propeller, four-cycle inflow, *U*=1 m/s, 600 rpm, 0.6R. (a) 90 deg; (b) 45 deg; (c) 0 deg.

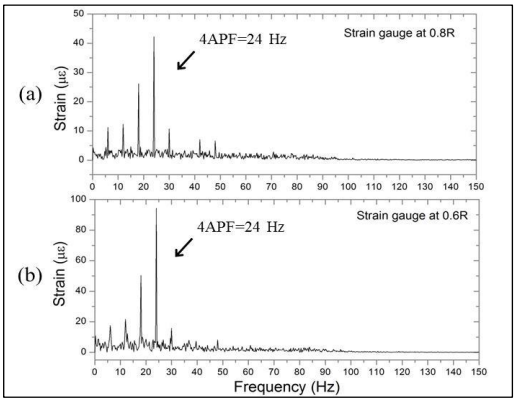

Figure 7. Strain frequency spectra at different radial locations, with plastic propeller, four-cycle inflow, U=0.5 m/s, 360 rpm. (a) 0.8R; (b) 0.6R.

3.4. Vibratory strain response with six-cycle wake screen

Figures 10 and 11 show the strain frequency spectra at multiple rotational speeds for the plastic and bronze propellers, respectively. The maximum peaks appear at 6APF which is in-line with the results obtained using the four-cycle inflow. The strong peak at 6APF corresponds to the heavy loading conditions that occur when the propeller blades pass through each of the six low axial velocity regions shown in Figure 4(b). A comparison between Figure 9(c) and Figure 10(c) shows that the peak amplitude of 4APF is approximately 3 times larger than that of 6APF for the same operating condition. This suggests that the single blade force of 4APF is larger than that of 6APF for the same tunnel speed and rotational speed.

4.Conclusions

An experimental study on the dynamic strain response of propeller blades interacting with cyclic inflows has been conducted. Two 7-bladed highly skewed model propellers of identical geometries, but different elastic characteristics were operated in four-cycle and six-cycle inflows to study the dynamic strain response. LDV measurements show that the wake screens

were successful at generating the four-cycle and six-cycle inflows with large enough amplitudes to produce measurable response. For the case of uniform inflow, the dominant frequency of the vibratory strain response occurs at the APF and its harmonics. These peaks may be produced by imbalances in any part of the system such as in the propeller or the shaft or any hydrodynamic non-uniformity. For the case of the four-cycle inflow, the small peaks at APF and its harmonics were still evident, however the maximum peak occurs at 4APF. The strong peak at 4APF corresponds to the heavy loading conditions induced by the propeller rotating through the four low axial velocity regions of the inflow. The three strain gauges (0 degrees, 45 degrees and 90 degrees) have the same frequency characteristics and the 45 degree strain gauge has the maximum amplitude. The strain gauges at 0.6R and 0.8R also have the same frequency characteristics. However, the amplitude at 0.6R is approximately twice as large as the amplitude at 0.8R. In the case of the six-cycle inflow, the maximum peaks occur at 6APF which corresponds to the heavy loading conditions caused by the propeller rotating through the six low axial velocity regions of the inflow. The peak strain measured for the six cycle inflow was approximately three times smaller than that measure due to the four cycle inflow.

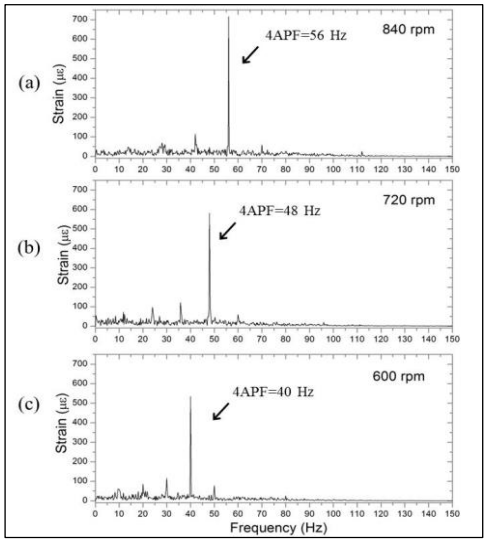

Figure 8. Strain frequency spectra with plastic propeller, four-cycle inflow, U=1.5 m/s. (a) 840 rpm; (b) 720 rpm; (c) 600 rpm.

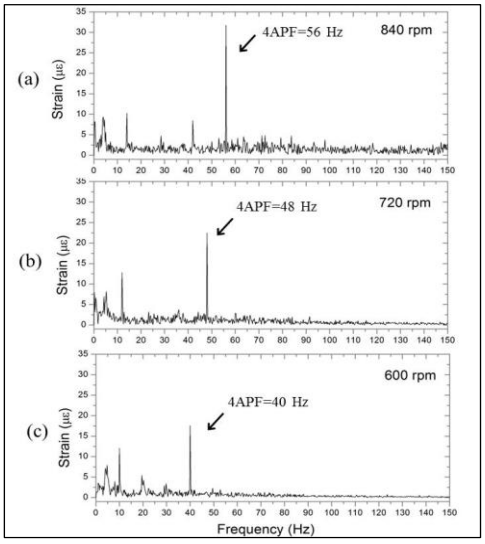

Figure 9. Strain frequency spectra with bronze propeller, four-cycle inflow, U=1.5 m/s. (a) 840 rpm; (b) 720 rpm; (c) 600 rpm.

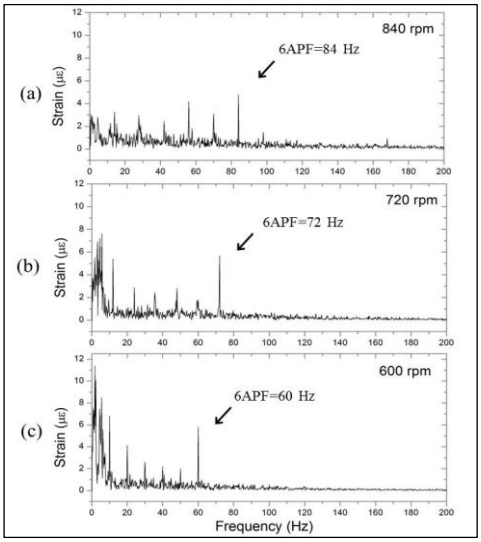

Figure 10. Strain frequency spectra with bronze propeller, six-cycle inflow, *U*=1.5 m/s. (a) 840 rpm; (b) 720 rpm; (c) 600 rpm.

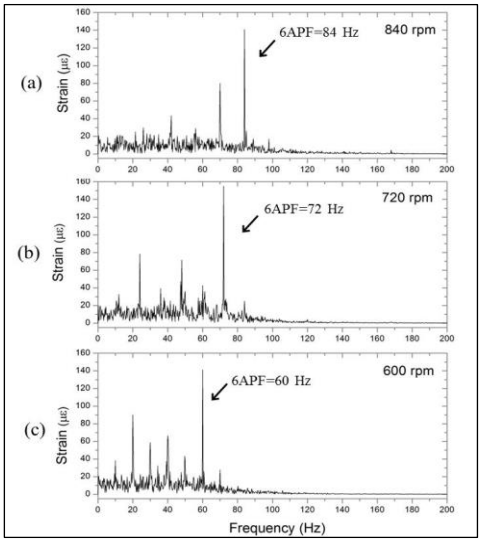

Figure 11. Strain frequency spectra with plastic propeller, six-cycle inflow, *U*=1.5 m/s. (a) 840 rpm; (b) 720 rpm; (c) 600 rpm.

Reference

[1] Zetterlind III VE, Watkins SE, Spoltman MW 2003 Fatigue testing of a composite propeller blade using fiber-optic strain sensors *Sensors Journal, IEEE.* **3** 393-9

[2] Seaver M, Trickey ST, Nichols JM 2006 Strain measurements from FBGs embedded in rotating composite propeller blades *Optical Fiber Sensors.* ThD2

[3] Liu Y, Lacher A, Wang G, Purekar A, Yu M 2007 Wireless fiber optic sensor system for strain and pressure measurements on a rotor blade *Optics East 2007.* 67700Y-Y-12

[4] Swithenbank SB, Jessup S, Etebari A 2008 Measurement of Crashback Loads on a Blade of Propeller 4381 in an Open and Ducted Configuration in the 36-inch Water Tunnel *Naval Surface Warfare Center Report.*

[5] Shin CS, Chen BL, Cheng JR, Liaw SK 2010 Impact Response of a Wind Turbine Blade Measured by Distributed FBG Sensors *Mater. Manuf. Process.* **25** 268-71

[6] Carr J, Baqersad J, Niezrecki C, Avitabile P, Slattery M. 2012 Dynamic stress–strain on turbine blade using digital image correlation techniques part 1: static load and calibration. *Topics in Experimental Dynamics Substructuring and Wind Turbine Dynamics, Volume 2* (New York: Springer) p 215-20.

[7] Carr J, Baqersad J, Niezrecki C, Avitabile P, Slattery M. 2012 Dynamic stress–strain on turbine blades using digital image correlation techniques part 2: dynamic measurements. *Topics in Experimental Dynamics Substructuring and Wind Turbine Dynamics, Volume 2* (New York:Springer) p 221-6.

[8] Carr J, Baqersad J, Niezrecki C, Avitabile P, Slattery M. 2013 Predicting dynamic strain on wind turbine blade using digital image correlation techniques in conjunction with analytical expansion methodologies. *Special Topics in Structural Dynamics, Volume 6* (New York:Springer) p 295-302.

[9] Kammerer A, Abhari RS 2009 Experimental Study on Impeller Blade Vibration During Resonance—Part I: Blade Vibration Due to Inlet Flow Distortion *Journal of Engineering for Gas Turbines and Power.* **131** 022508

[10] Kammerer A, Abhari RS 2009 Experimental Study on Impeller Blade Vibration During Resonance—Part II: Blade Damping *Journal of Engineering for Gas Turbines and Power.* **131** 022509

[11] Jessup SD 1990 Measurement of multiple blade rate unsteady propeller forces *David Taylor Research Center Report.*

[12] Liefvendahl M, Tröeng C 2011 Computation of cycle-to-cycle variation in blade load for a submarine propeller using LES *Proc Second International Symposium on Marine Propulsors.*

[13] Wei Y, Wang Y 2013 Unsteady hydrodynamics of blade forces and acoustic responses of a model scaled submarine excited by propeller's thrust and side-forces *J. Sound. Vib.* **332** 2038-56